Inferring Geyser Fountain Geometry from Electrical Measurements / Electric Field Response to Geyser Fountain Dynamics

Julia E. Gestrich[1*], Corrado Cimarelli[1], Alec J. Bennett[2], Antonio Capponi[1], Silvi Klein Schiphorst[3], Carina Poetsch[1]

[1*]Department of Earth and Environmental Sciences, Ludwig-Maximilians-Universität München, Theresienstrasse 41, München, 80333, Germany.
[2]Department, Senseca UK, Bristol, United Kingdom, Unit 8 Harbour Road Trading Estate, Portishead, Bristol, BS20 7BL, United Kingdom.
[3]Department of Earth Sciences, Utrecht University, Heidelberglaan 8, Utrecht, 3584 CS, The Netherlands.

*Corresponding author(s). E-mail(s): julia.gestrich@gmail.com;
Contributing authors: cimarelli@lmu.de; alec.bennett@senseca.com;
antonio.capponi@min.uni-muenchen.de;
s.kleinschiphorst@students.uu.nl; Carina.Poetsch@lmu.de;

S1 EFM Data Quality

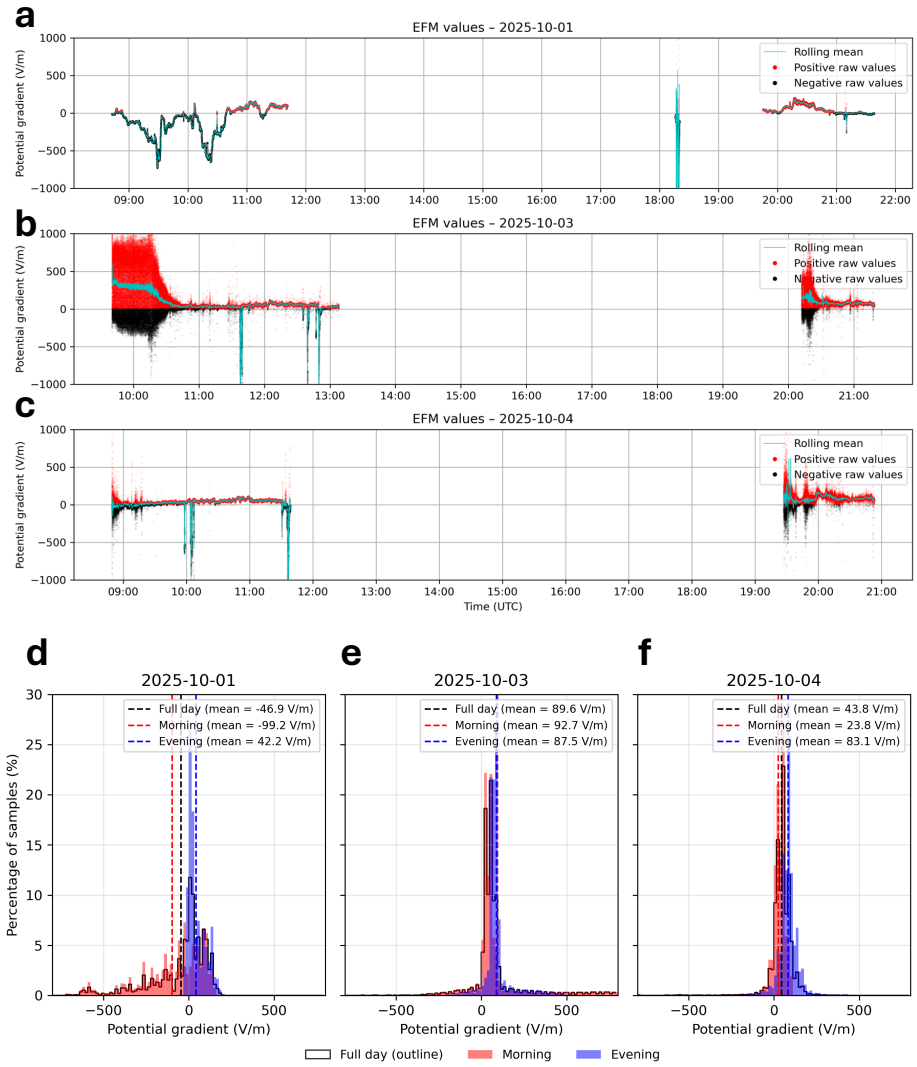

Fig. S1 EFM measurements of the potential gradient at Strokkur Geyser for October 1 (a) with histogram of values in (d), October 3 (b) with histogram (e), and October 4 (c) with histogram in (f). In (a)-(c), red dots show positive PG values while black dots show negative values. The histograms in (d)-(f) display the morning data for each day in red and the evening data in blue, with a black outline indicating the total histogram for each day. Vertical dashed lines in the corresponding colors indicate the mean value for each day, labeled in the legend.

S2 FEMM Model Details

S2.1 Geometrical Correction

As the FEMM model is 3D axisymmetric, we define the boundaries, conductors, and materials in a 2D plane that is rotated around the left-hand y-axis. We draw the geyser fountain parallel to the symmetry axis to achieve a cylindrical fountain shape. In reality, the BTD has a spherical antenna (0.2 m diameter) that we draw at a distance r_{BTD} from the fountain. However, due to the axisymmetry, the BTD is modeled as a torus surrounding the fountain, leading to a larger induced charge than a spherical conductor would. We correct for the geometry by calculating a conversion factor that can be applied to the torus's induced charge to estimate the induced charge on a realistic spherical conductor. We first calculate the induced charge of the torus using a set potential gradient without any fountain at r_{BTD} and with a maximum BTD height of h_{BTD} (Figure S2 (a)). Then, we move the entire BTD setup to be centered at the symmetry axis, resulting in a spherical conductor shape (Figure S2 (b)). Dividing the induced charge of the torus by the induced charge of the sphere gives us the torus-to-sphere geometric correction factor c_{tts}. This factor depends on the potential gradient, the height of the BTD, and its distance from the symmetry axis, and must be recalculated if these parameters change. All values of induced charge in the paper are already corrected for the geometry by dividing the raw induced charge output by c_{tts}.

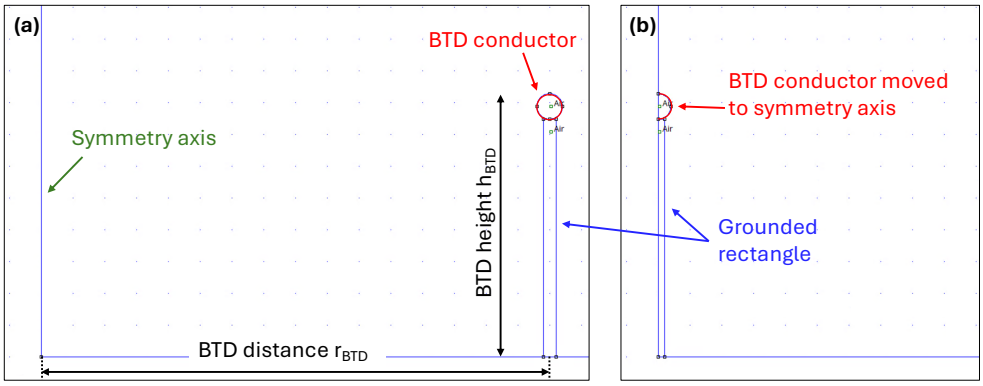

Fig. S2 FEMM 4.1 setup regarding the BTD placement and parameters. (a) BTD at modeled distance r_{BTD} to the symmetry axis on the left with a total height of h_{BTD} and a circular conductor with a diameter of 0.2 m. (b) BTD moved to the symmetry axis to calculate the torus-to-sphere correction factor. Note that in panels (a) and (b), the "Air" tags indicate that all polygons are assigned the resistivity of air. It does not affect the model as the boundaries are set to a fixed voltage.

S2.2 BTD Height Sensitivity

The induced charge on the BTD by the height variations of the fountain is dependent on the height of the BTD conductor above ground. Although we did not vary the height between the measurements of the geyser fountains during field observation, changes in the conductor height in a future campaign would need to be accounted for to make the measurements comparable. We calculate the induced charge for BTD heights between 1 - 2.2 m for different fountain heights and radii and compare the results to the default BTD height of 2.07 m. We leave other parameters at their default values and the potential gradient at PG=100 V/m. We can see in Figure S3 (a), that the absolute induced charge is proportional to the BTD height and independent of the fountain height, with higher BTD heights showing a higher absolute induced charge. Figure S3 (b) and (d), shows that by moving the BTD ±1 m, the induced charge doubles or halves. This relationship is also independent of the fountain radius.

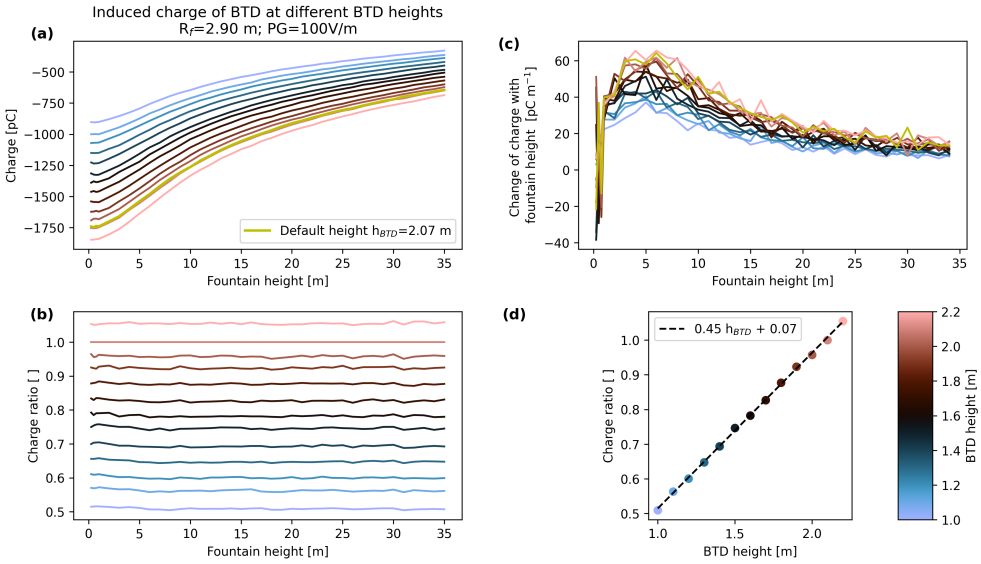

Fig. S3 (a) Influence of BTD antenna height (different colors in colorbar) on the modeled induced charge for a fountain radius of 2.9 m. The yellow line shows the charge of the default height 2.07 m. (b) Ratio between the induced charge at different BTD heights and the induced charge at the default height of h_{BTD}=2.07 m. (c) Slope of the charge with fountain height. (d) Average ratios of (b) over all fountain heights per BTD height.

S2.3 BTD Distance Sensitivity

Similar to the sensitivity analysis regarding the BTD height, we now evaluate the sensitivity towards the distance between the BTD and the center of the fountain. As before, we leave all other parameters at their default value, also the BTD height at 2.07 m, and only vary the distance r_{BTD} between 5 - 15.5 m and compare the result

to that using the default distance during the field campaign of r_{BTD}=9 m. Unlike the sensitivity to the BTD height, the distance between the BTD and the fountain does not influence the induced charge at 0 m fountain height. This is expected because the atmospheric potential gradient is uniform and independent of the BTD's lateral location. However, as the fountain height increases, the induced charge varies significantly with distance. For example, positioning a BTD very close to a fountain (e.g. at 5 m distance) with a fountain radius of 2.9 m, the induced charge rises very quickly for fountain heights below 5 m and then flattens, meaning the change in fountain height leads to a smaller change in induced charge for higher fountains (Figure S4 (b)). Conversely, a BTD at larger distances (e.g. 15 m) experiences a very gradual, slowly rising induced charge. This means that the BTD distance changes the slope of charge with fountain height (Figure S4 (d)). This effect is stronger for large fountain radii and smaller for small fountain radii (Figure S4 (a) and (c) compared to (b) and (d)).

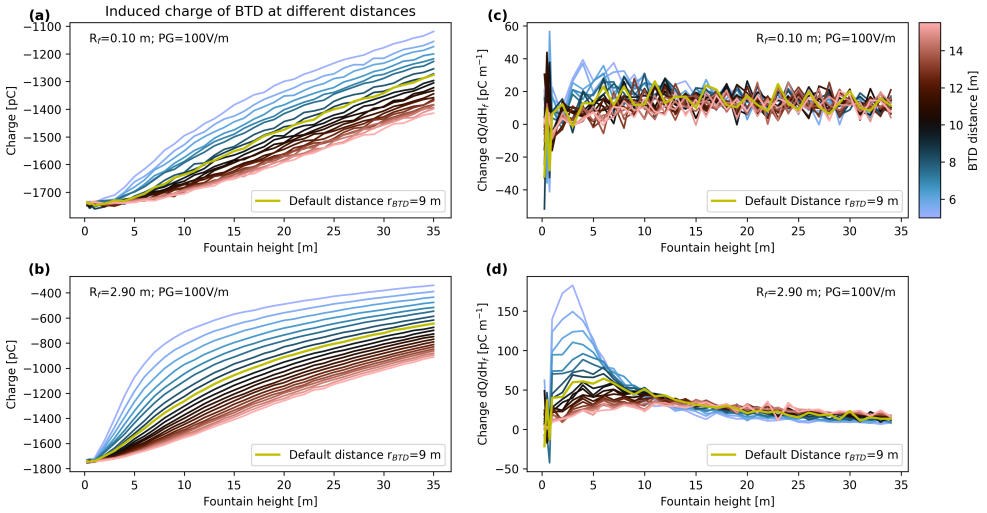

Fig. S4 (a) Influence of the distance between BTD and the fountain center (colors according to colorbar) and the induced charge on the BTD as a function of fountain height in comparison to the induced charge at the default distance of r_{BTD}=9 m (yellow line) for a fountain radius of R_f=0.1 m. (b) same as (a) but for a fountain radius of 2.9 m. (c) Slope of induced charge with fountain height in (a). (d) Slope of charge with fountain height in (b).

S2.4 Influence of Fountain Disruption

To investigate the effect of a disruption of the continuous fountain, we model the induced charge for additional scenarios where the fountain is made of spheres with an equal radius as the fountain that carry the charge of the ground (0 V) and ground-connected fountain, with various spacings in between the spheres (S5 (a)). This is a simplification of the possible disruption within a fountain, as it would more likely break into parts of different lengths and varying connectivity, with varying spacings

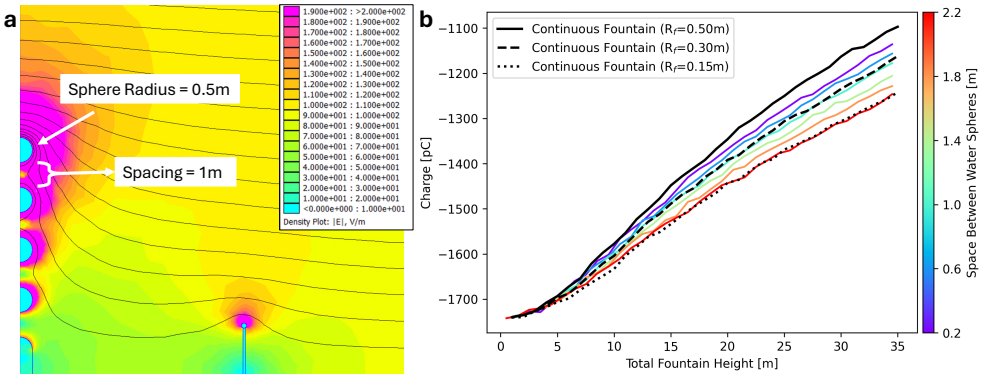

Fig. S5 (a) FEMM modeling setup for PG=100 V/m and R_f=0.5 m with spheres of the same radius and a spacing of 1 m. (b) Resulting induced charge per fountain height for different spacings between 0.2 m to 2.2 m (corresponding to different colors in the colorbar) between spheres of 0.5 m radius. As a comparison, the black line shows the induced charge for a continuous fountain of the same radius as the disrupted fountain (R_f=0.5 m), while the dashed and dotted black lines show the result for more narrow fountains of R_f=0.2 m and R_f=0.1 m.

within a single fountain. The fountain's actual disruption is not visible in the videos due to the spray surrounding it. We are unable to model the effect of the spray itself on the induced charge due to the axisymmetric model geometry. Additionally, small water droplets might lose their ground charge more quickly, another parameter we are unable to model here. However, the presented analysis provides a qualitative example and an idea of the effect of disruption on the induced charge. Figure S5 (b), shows that the difference between the continuous fountain with a radius of 0.5 m and the disrupted fountain of the same radius increases with fountain height, similar to the effect of the fountain radius. Even a small separation between the disconnected spheres of 0.2 m leads to a decrease in induced charge of approximately 40 pC at a fountain height of 35 m. This is due to a lower average fountain radius when assuming stacked spheres rather than a cylinder. The spacing of 1 m between the spheres induces a current comparable to a continuous fountain with a radius of 0.3 m. A spacing of 2.2 m corresponds to a continuous fountain with a radius of 0.15 m. However, we consider a spacing of more than 1 m between the larger connected parts of the fountain to be an extreme case that we do not observe in the videos.

S2.5 Approximating the empirical parameters

To approximate an empirical equation calculating the charge for a specific fountain height that is true for a range of potential gradients and fountain radii for our instrument geometry, we fit the sigmoid function of Equation **??** to each of the discrete FEMM solutions. We vary between 15 different fountain radii R_f (0.1 – 2.9 m) and 11 different potential gradients PG (10 – 510 V/m) and fit the equation to the charges calculated for each fountain height $Q(H_f)$ for each combination of R_f and PG. For the fitting, we use the *scipy.curve_fit* function in Python and invert for the parameters in the sigmoid curve Equation **??** h_s, k, m, and Q_0 (see Figure S6). The parameter h_s

is independend of PG and has a linear relationship to R_f, while k_s is approximately constant

$$h_s(R_f) = -5.52 \cdot R_f + 17.26\,\mathrm{m} \tag{1}$$
$$k_s \approx 0.096\,\mathrm{m}^{-1}. \tag{2}$$

On the other hand, the parameters m_s and Q_0 are dependent on both PG and R_f as shown in Figure S6 (c) and (d). We first fit a second-degree polynomial to the lines showing the dependence of m_s or Q_0 on the radius R_f for each potential gradient PG

$$m_s(R_f, PG) = p_{m,0}(PG) \cdot R_f^2 + p_{m,1}(PG) \cdot R_f + p_{m,2} \tag{3}$$
$$Q_0(R_f, PG) = p_{Q,0}(PG) \cdot R_f^2 + p_{Q,1}(PG) \cdot R_f + p_{Q,2}. \tag{4}$$

Subsequently, we analyze the polynomial parameters $(p_{i,0}, p_{i,1}, p_{i,2})$ for their dependence on PG and find linear relationships for each of them

$$p_{m,0}(PG) = 0.55\,\mathrm{V}^{-1} \cdot PG; \quad p_{m,1} = 3.85\,\mathrm{m\,V}^{-1} \cdot PG; \quad p_{m,2} = 7.15\,\mathrm{m}^2\,\mathrm{V}^{-1} \cdot PG; \tag{5}$$
$$p_{Q,0}(PG) = -1.03\,\mathrm{V}^{-1} \cdot PG; \quad p_{Q,1} = -0.40\,\mathrm{m\,V}^{-1} \cdot PG; \quad p_{Q,2} = -18.95\,\mathrm{m}^2\,\mathrm{V}^{-1} \cdot PG. \tag{6}$$

Inserting Eq. 5 in Eq. 3 and Eq. 6 in Eq. 4 we derive the equations for m_s and Q_0 as fuctions of PG and R_f (Eq. **??** and **??**).

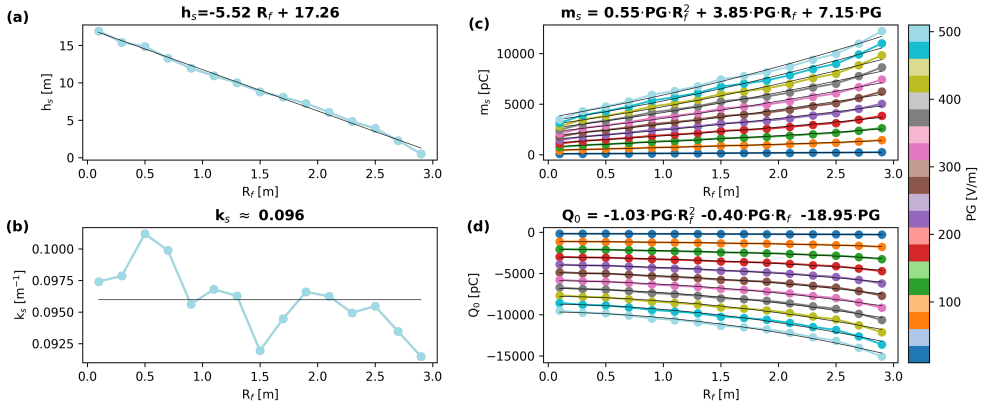

Fig. S6 Sigmoid equation parameter variation with the fountain radius R_f and potnetial gradient PG. The colored lines correspond to different PG. In (a) and (b), the lines all overlap, creating one single line showing that the parameter is independent of PG. The black lines show the parameter estimation according to the equations above each panel.

S3 Additional Figures for Results

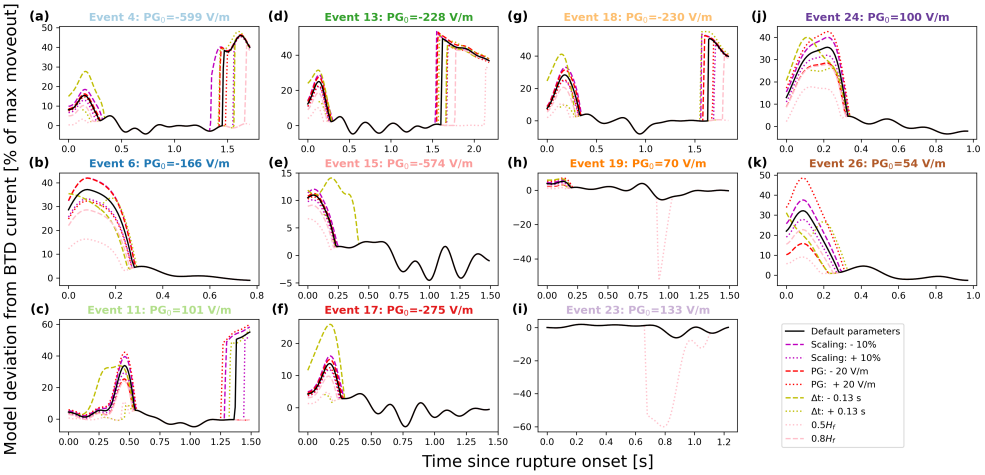

Fig. S7 Difference between modeled and BTD measured current expressed as percentage relative to the maximum BTD current moveout. (a) – (k) show the results for each event, labeled at the top of each panel. The percentage difference for the modeled current using default parameter values is shown in black, occasionally obscuring the other lines when they overlap. The effect of parameter uncertainties is shown as purple (video scaling), red (PG), and yellow (time shift) lines that are dashed for a decrease in the parameter by their uncertainty and dotted for an increase. The light pink lines show the effect of a decrease of the effective fountain height to 50% (dotted line) and 80% (dashed line) of the fountain top height. Axes for each panel have the same units.

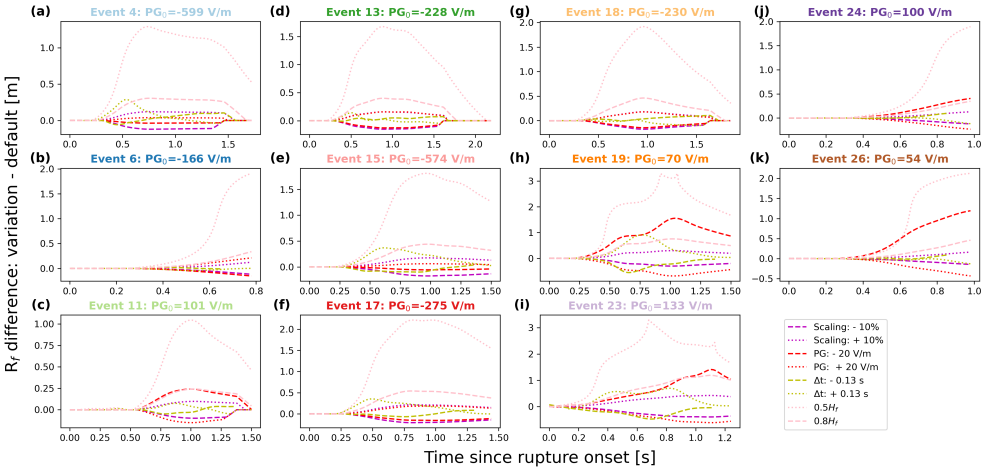

Fig. S8 Difference between the inverted fountain radius when applying the parameter uncertainties compared to the inverted fountain radius using the default parameters. (a) – (k) show the results for each event, labeled at the top of each panel. The effect of the different parameter uncertainties is shown by purple (video scaling), red (PG_0), and yellow (time shift) lines, which are dashed for a decrease in the parameter by its uncertainty and dotted for an increase. The light pink lines show the effect of a decrease of the effective fountain height to 50% (dotted line) and 80% (dashed line) of the fountain top height. Axes for each panel have the same units.

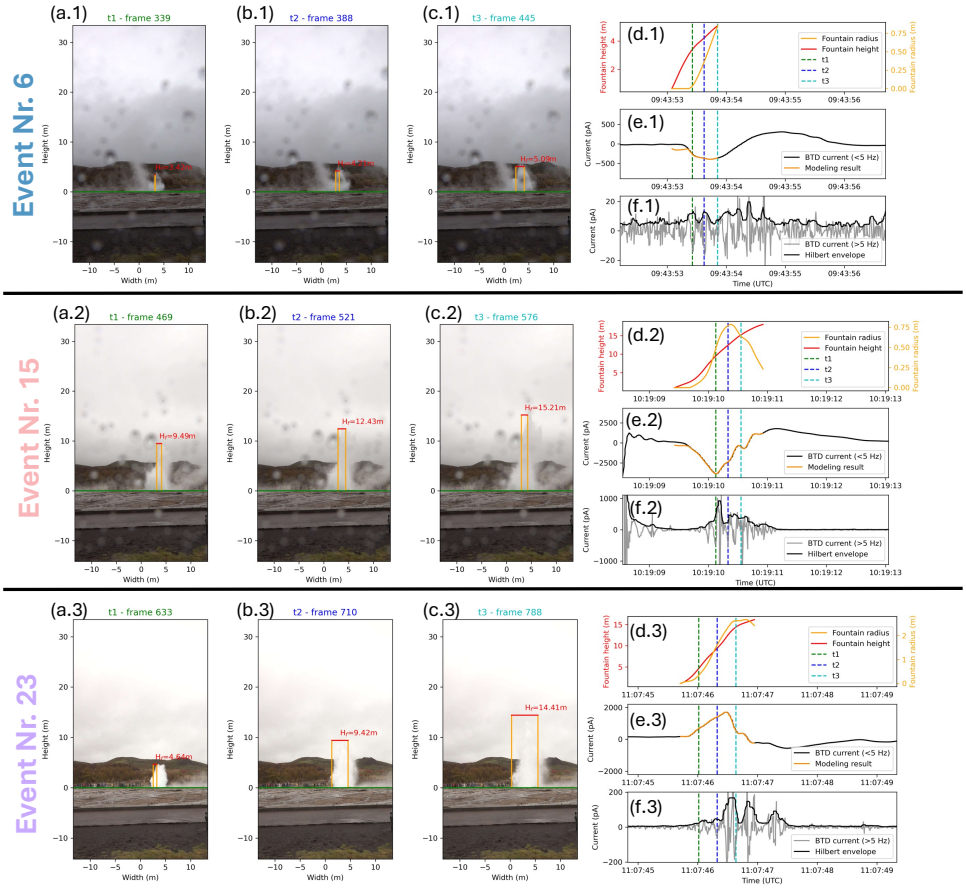

Fig. S9 Examples of fountain events Nr. 6 (x.1), 15 (x.2), and 23 (x.3) and their fountain radius inversion results with time. For each event, there are 6 panels (labeled for example (a.1) – (a.6)) with the first three panels (a) – (c) showing the video frames at different times t0, t1, and t2. Additionally, the fountain height H_f is indicated by a red horizontal bar, and the fountain extends based on the inverted radius R_f, indicated by orange vertical lines. (d) shows the tracked fountain height in red and the inverted fountain radius in orange with vertical dashed lines showing the timing of the frames in the first three panels: t0 (green), t1 (blue), and t2 (lightblue). These vertical lines also exist for (e) and (f). (e) shows the low-frequency BTD current (black) and the modeled current fit (orange). (f) shows the high-frequency BTD current (grey) with the Hilbert Transform Envelope (black).